

A dimensional decomposition method for stochastic fracture mechanics

Sharif Rahman *

Department of Mechanical and Industrial Engineering, The University of Iowa, Iowa City, IA 52242, United States

Received 13 November 2005; received in revised form 17 April 2006; accepted 17 April 2006

Available online 19 June 2006

Abstract

This paper presents a new dimensional decomposition method for obtaining probabilistic characteristics of crack-driving forces and reliability analysis of general cracked structures subject to random loads, material properties, and crack geometry. The method involves a novel function decomposition permitting lower-variate approximations of a crack-driving force or a performance function, Lagrange interpolations for representing lower-variate component functions, and Monte Carlo simulation. The effort required by the proposed method can be viewed as performing deterministic fracture analyses at selected input defined by sample points. Compared with commonly-used first- and second-order reliability methods, no derivatives of fracture response are required by the new method developed. Results of three numerical examples involving both linear-elastic and nonlinear fracture mechanics of cracked structures indicate that the decomposition method provides accurate and computationally efficient estimates of probability density of the J -integral and probability of fracture initiation for various cases including material gradation characteristics and magnitudes of applied stresses and loads.

© 2006 Elsevier Ltd. All rights reserved.

Keywords: Probability density of J -integral; Probability of fracture initiation; Decomposition method; Univariate decomposition; Bivariate decomposition

1. Introduction

Stochastic fracture mechanics (SFM) is concerned with characterizing statistical uncertainties in loads, material properties, and geometry and quantifying their impact on fracture response and integrity of materials and structures. SFM, which blends the classical fracture mechanics and the probability theory, accounts for both mechanistic and statistical aspects of the crack-driving force and provides probabilistic characteristics of fracture initiation and growth of an existing crack, real or postulated, in an engineering structure. The implementation of SFM allows a rational way of incorporating and managing statistical uncertainties in engineering

* Tel.: +1 319 335 5679; fax: +1 319 335 5669.

E-mail address: rahman@engineering.uiowa.edu

URL: <http://www.engineering.uiowa.edu/~rahman>

design and analysis. As a result, SFM finds applications in many engineering disciplines today as diverse as aerospace and aircraft propulsion, civil infrastructure, electronic packaging, oil and gas industry, geology, nuclear piping and pressure vessels, automotive systems, off-shore and marine industry, and others.

The most common probabilistic methods employed in SFM are perhaps the first- and second-order reliability methods (FORM/SORM) [1–3] and simulation methods [4–6]. FORM/SORM is based on linear (FORM) or quadratic approximation (SORM) of the limit-state surface at a most probable point (MPP). The MPP can be located by various gradient-based optimization algorithms, which in turn require first- and/or second-order response sensitivities or gradients, for which efficient means of calculation are required. If these sensitivities of fracture response can be calculated analytically, FORM and SORM are quite efficient [7–9]. Otherwise, FORM/SORM can be ineffective, for instance, when response sensitivities are not available or when sensitivity analysis is computationally intensive. In addition, for highly nonlinear performance functions, which exist in many fracture problems, results based on FORM/SORM must be interpreted with caution. If the Rosenblatt transformation, frequently used to map non-Gaussian random input into its standard Gaussian image, yields a highly nonlinear limit state, inadequate reliability estimates by FORM/SORM may result. The *simulation methods* involving sampling and estimation are well known in the statistics and reliability literature. Direct Monte Carlo simulation [4] is the most widely used simulation method, generally requires a large number of simulations to calculate low failure probability, and is impractical when each simulation involves expensive finite-element, boundary-element, or mesh-free calculations. While simulation methods do not exhibit the limitations of approximate reliability methods, such as FORM/SORM, they generally require extensive calculations than the former methods. Consequently, simulation methods have been traditionally employed as a measuring stick for approximate methods.

This paper presents a new class of computational methods, referred to as the dimensional decomposition method, for predicting probabilistic characteristics of fracture response and reliability of engineering structures subject to random loads, material properties, and geometry. The method involves a novel function decomposition allowing lower-variate approximations of fracture response, Lagrange interpolations for representing various component functions, and efficient Monte Carlo simulation. Section 2 describes random parameters and their impact on propagating uncertainties to fracture response. Section 3 gives a brief exposition of a function decomposition that facilitates its lower-dimensional approximations. Section 4 describes how the function decomposition is exploited in solving a general probabilistic fracture-mechanics problem. Three numerical examples involving both linear-elastic and nonlinear fracture-mechanics problems illustrate the proposed method in Section 5. Comparisons have been made with alternative approximate and simulation methods to evaluate the accuracy and computational efficiency of the new method. Finally, Section 6 provides conclusions from this work.

2. Stochastic fracture response and failure criteria

2.1. Random parameters and fracture response

Let (Ω, \mathcal{F}, P) be a probability space, where Ω is the sample space, \mathcal{F} is the σ -algebra of subsets of Ω , and P is the probability measure, and \mathbb{R}^N be an N -dimensional real vector space. Defined on the probability space (Ω, \mathcal{F}, P) , let $\mathbf{X} = \{X_1, \dots, X_N\}^T \in \mathbb{R}^N$ denote an N -dimensional input random vector, which characterizes statistical uncertainties of *all* input parameters including loads, material properties, and geometry. For example, if the crack length $2a$, the crack orientation γ , random vectors \mathbf{X}_E and \mathbf{X}_v respectively representing gradation characteristics of elastic modulus and Poisson's ratio, and M external loads S_1, \dots, S_M are modeled as input random variables in fracture analysis of a linear-elastic and isotropic functionally graded material, then $\mathbf{X} = \{2a, \gamma, \mathbf{X}_E, \mathbf{X}_v, S_1, \dots, S_M\}^T$. Similarly, if the crack length $2a$, tensile properties E , α , and m , and M external loads S_1, \dots, S_M are stochastic variables in nonlinear fracture analysis of a homogeneous media, then $\mathbf{X} = \{2a, E, \alpha, m, S_1, \dots, S_M\}^T$. If some of these random parameters have a spatial variability, they are typically modeled as random fields, which must be discretized into a countable number of random variables to create \mathbf{X} . Regardless, the input random vector $\mathbf{X} \in \mathbb{R}^N$ including all relevant sources of uncertainties must be characterized by its joint probability density function $f_{\mathbf{X}}(\mathbf{x}) : \mathbb{R}^N \mapsto \mathbb{R}$. However, in most practical applications, complete information required to derive the joint probability density may not be available. In that case, one commonly

invokes the assumption of statistical independence among random variables or employs a judiciously chosen joint distribution property in conjunction with observed second-moment characteristics (e.g., covariance matrix) to describe the joint density of \mathbf{X} .

A major objective of SFM is to find probabilistic characteristics of crack-driving forces, such as stress-intensity factors (SIFs) $K_i(\mathbf{X})$, $i = \text{I, II, and III}$ for all three modes (e.g., in linear-elastic analysis), the J -integral $J(\mathbf{X})$ (e.g., in linear-elastic or nonlinear-elastic analysis), and other fracture integrals due to uncertain input \mathbf{X} . Let $y(\mathbf{X})$ describe a generic crack-driving force or a relevant performance function involving the crack-driving force for a given fracture problem of interest. In general, the multivariate function $y(\mathbf{x}) : \mathbb{R}^N \mapsto \mathbb{R}$ is implicit, is not analytically available, and can only be viewed as a high-dimensional input–output mapping, where the evaluation of the output function y for a given input \mathbf{x} requires expensive finite-element, boundary element, or mesh-free analysis. Therefore, methods employed in SFM analysis must be capable of generating accurate probabilistic characteristics of $y(\mathbf{X})$ with an acceptably small number of output function evaluations.

2.2. Failure criteria

Consider SIFs K_i , $i = \text{I, II, and III}$ and the J -integral for a crack tip that can be calculated using standard finite element analysis (FEA) for a given input. Suppose that a failure is defined when the crack propagation is initiated at that crack tip, i.e., when $K_{\text{eff}} \equiv h(K_{\text{I}}, K_{\text{II}}, K_{\text{III}}) > K_{\text{Ic}}$ or $J > J_{\text{Ic}}$, where K_{eff} is an effective SIF with h depending on a selected mixed-mode theory, and K_{Ic} or J_{Ic} is a relevant mode-I fracture toughness of the material measured in terms of SIF or J -integral. This requirement cannot be satisfied with certainty, since K_i or J is dependent on the input vector \mathbf{X} which is random, and K_{Ic} or J_{Ic} itself may be a random variable. Hence, the performance of the cracked structure should be evaluated by the reliability or its complement, the probability of failure P_{F} , defined as the multi-fold integral

$$P_{\text{F}} \equiv P[y(\mathbf{X}) < 0] \equiv \int_{y(\mathbf{x}) < 0} f_{\mathbf{X}}(\mathbf{x}) d\mathbf{x}, \quad (1)$$

where

$$y(\mathbf{X}) = \begin{cases} K_{\text{Ic}}(\mathbf{X}) - K_{\text{eff}}(\mathbf{X}), & \text{SIF-based analysis} \\ J_{\text{Ic}}(\mathbf{X}) - J(\mathbf{X}), & \text{J-based analysis} \end{cases} \quad (2)$$

is a multivariate performance function that depends on random input \mathbf{X} . The evaluation of the multi-dimensional integral, either analytically or numerically, is not possible because N is large, $f_{\mathbf{X}}(\mathbf{x})$ is generally non-Gaussian, and $y(\mathbf{x})$ is a highly nonlinear function of \mathbf{x} . Direct Monte Carlo simulation is impractical for calculating small failure probabilities since the evaluation of $y(\mathbf{x})$ entails expensive numerical computation.

Eq. (1) represents the probability of initiation of crack growth, which provides a conservative estimate of structural performance. A less conservative evaluation requires calculating the probability when crack growth, if occurs, is unstable. The latter probability, known as the probability of fracture instability, is more difficult to compute, since it must be obtained by incorporating automatic crack-growth simulation in a stochastic fracture-mechanics analysis. Furthermore, knowledge of the derivatives of crack-driving force with respect to crack-size parameters is required. In the past, the author examined probabilities of both fracture initiation and instability of circumferentially cracked cylinders, for which simple, empirically-derived handbook solutions of J -integral are readily available [10]. However, for a general cracked structure, no such handbook solutions exist; one must conduct expensive FEA to obtain crack-driving force and its derivatives to be integrated with a stochastic analysis. Therefore, calculating the probability of fracture instability of a general cracked structure is not a trivial effort. In this work, all probabilistic calculations are limited to the fracture initiation, although any performance function describing input–output system behavior is applicable.

3. Multivariate function decomposition

Consider a continuous, differentiable, real-valued function $y(\mathbf{x}) : \mathbb{R}^N \mapsto \mathbb{R}$ that depends on $\mathbf{x} = \{x_1, \dots, x_N\}^T \in \mathbb{R}^N$. A dimensional decomposition of $y(\mathbf{x})$, described by [11–13]

$$y(\mathbf{x}) = y_0 + \underbrace{\sum_{i=1}^N y_i(x_i)}_{=\hat{y}_1(\mathbf{x})} + \underbrace{\sum_{\substack{i_1, i_2=1 \\ i_1 < i_2}}^N y_{i_1 i_2}(x_{i_1}, x_{i_2}) + \dots + \sum_{\substack{i_1, \dots, i_S=1 \\ i_1 < \dots < i_S}}^N y_{i_1 \dots i_S}(x_{i_1}, \dots, x_{i_S}) + \dots + y_{12 \dots N}(x_1, \dots, x_N)}_{=\hat{y}_2(\mathbf{x})} \dots \underbrace{\dots}_{=\hat{y}_S(\mathbf{x})} \quad (3)$$

can be viewed as a finite hierarchical expansion of an output function in terms of its input variables with increasing dimensions, where y_0 is a constant, $y_i(x_i) : \mathbb{R} \mapsto \mathbb{R}$ is a univariate component function representing individual contribution to $y(\mathbf{x})$ by input variable x_i acting alone, $y_{i_1 i_2}(x_{i_1}, x_{i_2}) : \mathbb{R}^2 \mapsto \mathbb{R}$ is a bivariate component function describing cooperative influence of two input variables x_{i_1} and x_{i_2} , $y_{i_1 \dots i_S}(x_{i_1}, \dots, x_{i_S}) : \mathbb{R}^S \mapsto \mathbb{R}$ is an S -variate component function quantifying cooperative effects of S input variables x_{i_1}, \dots, x_{i_S} , and so on. The last term in Eq. (3) represents any residual dependence of all input variables cooperatively locked together to affect the output function y . If

$$\hat{y}_S(\mathbf{x}) = y_0 + \sum_{i=1}^N y_i(x_i) + \sum_{\substack{i_1, i_2=1 \\ i_1 < i_2}}^N y_{i_1 i_2}(x_{i_1}, x_{i_2}) + \dots + \sum_{\substack{i_1, \dots, i_S=1 \\ i_1 < \dots < i_S}}^N y_{i_1 \dots i_S}(x_{i_1}, \dots, x_{i_S}) \quad (4)$$

represents a general S -variate approximation of $y(\mathbf{x})$, the univariate ($S = 1$) and bivariate ($S = 2$) approximations, respectively denoted by $\hat{y}_1(\mathbf{x})$ and $\hat{y}_2(\mathbf{x})$, provide two- and three-term approximants of the finite decomposition in Eq. (3). Similarly, trivariate, quadrivariate, and other higher-variate approximations can be derived by appropriately selecting the value of S . The fundamental conjecture underlying this work is that component functions arising in the function decomposition will exhibit insignificant S -variate effects cooperatively when $S \rightarrow N$, leading to useful lower-variate approximations of $y(\mathbf{x})$. In the limit, when $S = N$, $\hat{y}_S(\mathbf{x})$ converges to the exact function $y(\mathbf{x})$. In other words, Eq. (4) generates a hierarchical and convergent sequence of approximations of $y(\mathbf{x})$.

4. Dimensional decomposition method

4.1. Lower-variate approximations based on a reference point

For a probabilistic fracture problem, recall that $y(\mathbf{x}) \equiv y(x_1, \dots, x_N)$ represents either a crack-driving force (e.g., SIF, J -integral, etc.) or a performance function that depends on crack-driving force (e.g., Eq. (2)). In either case, consider univariate and bivariate approximations of $y(\mathbf{x})$, respectively defined by

$$\hat{y}_1(\mathbf{x}) \equiv \hat{y}_1(x_1, \dots, x_N) \equiv \sum_{i=1}^N \underbrace{y(c_1, \dots, c_{i-1}, x_i, c_{i+1}, \dots, c_N)}_{=y_i(x_i)} \underbrace{-(N-1)y(\mathbf{c})}_{=y_0} \quad (5)$$

and

$$\hat{y}_2(\mathbf{x}) \equiv \hat{y}_2(x_1, \dots, x_N) \equiv \sum_{\substack{i_1, i_2=1 \\ i_1 < i_2}}^N \underbrace{y(c_1, \dots, c_{i_1-1}, x_{i_1}, c_{i_1+1}, \dots, c_{i_2-1}, x_{i_2}, c_{i_2+1}, \dots, c_N)}_{=y_{i_1 i_2}(x_{i_1}, x_{i_2})} + \sum_{i=1}^N \underbrace{-(N-2)y(c_1, \dots, c_{i-1}, x_i, c_{i+1}, \dots, c_N)}_{=y_i(x_i)} + \underbrace{\frac{(N-1)(N-2)}{2}y(\mathbf{c})}_{=y_0} \quad (6)$$

where $\mathbf{c} = \{c_1, \dots, c_N\}^T$ is a reference point in the input domain, $y(\mathbf{c}) \equiv y(c_1, \dots, c_N)$, $y_i(x_i) \equiv y(c_1, \dots, c_{i-1}, x_i, c_{i+1}, \dots, c_N)$, $y_{i_1 i_2}(x_{i_1}, x_{i_2}) \equiv y(c_1, \dots, c_{i_1-1}, x_{i_1}, c_{i_1+1}, \dots, c_{i_2-1}, x_{i_2}, c_{i_2+1}, \dots, c_N)$. Based on the author’s past experience, the mean point of random input defines a suitable reference point. Neverthe-

less, these two approximations of $y(\mathbf{x})$ can be generalized to an S -variate approximation for any integer $1 \leq S \leq N$, given by

$$\hat{y}_S(\mathbf{x}) \equiv \sum_{i=0}^S (-1)^i \binom{N-S+i-1}{i} \sum_{\substack{k_1, \dots, k_{S-i}=1 \\ k_1 < \dots < k_{S-i}}}^N y(c_1, \dots, c_{k_1-1}, x_{k_1}, c_{k_1+1}, \dots, c_{k_{S-i}-1}, x_{k_{S-i}}, c_{k_{S-i}+1}, \dots, c_N), \tag{7}$$

where $y(c_1, \dots, c_{k_1-1}, x_{k_1}, c_{k_1+1}, \dots, c_{k_{S-i}-1}, x_{k_{S-i}}, c_{k_{S-i}+1}, \dots, c_N)$ is an $(S - i)$ th dimensional component function representing $(S - i)$ th dimensional cooperation among input variables $x_{k_1}, \dots, x_{k_{S-i}}$. Using a multivariate function theorem proposed by Xu and Rahman [14], it can be shown that $\hat{y}_S(\mathbf{x})$ in Eq. (7) consists of all terms of the Taylor series of $y(\mathbf{x})$ that have less than or equal to S variables. The expanded form of Eq. (7), when compared with the Taylor expansion of $y(\mathbf{x})$, indicates that the residual error in the S -variate approximation is $y(\mathbf{x}) - \hat{y}_S(\mathbf{x}) = \mathcal{R}_{S+1}$, where the remainder \mathcal{R}_{S+1} includes terms of dimensions $S + 1$ and higher. When $S = 1$ and 2, Eq. (7) degenerates to univariate (Eq. (5)) and bivariate (Eq. (6)) approximations, respectively.

It is worth noting that the univariate or bivariate approximations should not be viewed as first- or second-order Taylor series expansions nor do they limit the nonlinearity of $y(\mathbf{x})$. In fact, all higher-order univariate or bivariate terms of $y(\mathbf{x})$ are included in Eq. (5) or (6), which therefore, should provide in general higher-order representation of a multivariate function than those by first- or second-order Taylor expansions.

4.2. Lagrange interpolations

Consider the univariate component function $y_i(x_i) \equiv y(c_1, \dots, c_{i-1}, x_i, c_{i+1}, \dots, c_N)$ in Eq. (5) or (6). If for sample points $x_i = x_i^{(j)}$; $j = 1, \dots, n$, n distinct function values $y(c_1, \dots, c_{i-1}, x_i^{(j)}, c_{i+1}, \dots, c_N)$; $j = 1, \dots, n$ are given, the function value for an arbitrary x_i can be obtained by the Lagrange interpolation

$$y_i(x_i) = \sum_{j=1}^n \phi_j(x_i) y(c_1, \dots, c_{i-1}, x_i^{(j)}, c_{i+1}, \dots, c_N), \tag{8}$$

where

$$\phi_j(x_i) = \frac{\prod_{k=1, k \neq j}^n (x_i - x_i^{(k)})}{\prod_{k=1, k \neq j}^n (x_i^{(j)} - x_i^{(k)})} \tag{9}$$

is the Lagrange shape function. By using Eqs. (8) and (9), arbitrarily many values of $y_i(x_i)$ can be generated if n values of that component function are given. The same idea can be applied to the bivariate component function $y_{i_1 i_2}(x_{i_1}, x_{i_2}) \equiv y(c_1, \dots, c_{i_1-1}, x_{i_1}, c_{i_1+1}, \dots, c_{i_2-1}, x_{i_2}, c_{i_2+1}, \dots, c_N)$ in Eq. (6). If for $x_{i_1} = x_{i_1}^{(j_1)}$ and $x_{i_2} = x_{i_2}^{(j_2)}$, n^2 function values $y_{i_1 i_2}(x_{i_1}^{(j_1)}, x_{i_2}^{(j_2)}) \equiv y(c_1, \dots, c_{i_1-1}, x_{i_1}^{(j_1)}, c_{i_1+1}, \dots, c_{i_2-1}, x_{i_2}^{(j_2)}, c_{i_2+1}, \dots, c_N)$; $j_1, j_2 = 1, \dots, n$ are given, the function value for an arbitrary point (x_{i_1}, x_{i_2}) can be obtained using the Lagrange interpolation

$$y_{i_1 i_2}(x_{i_1}, x_{i_2}) = \sum_{j_2=1}^n \sum_{j_1=1}^n \phi_{j_1}(x_{i_1}) \phi_{j_2}(x_{i_2}) y(c_1, \dots, c_{i_1-1}, x_{i_1}^{(j_1)}, c_{i_1+1}, \dots, c_{i_2-1}, x_{i_2}^{(j_2)}, c_{i_2+1}, \dots, c_N). \tag{10}$$

The same procedure is repeated for all univariate and bivariate component functions, i.e., for all $y_i(x_i)$, $i = 1, \dots, N$ and for all $y_{i_1 i_2}(x_{i_1}, x_{i_2})$, $i_1, i_2 = 1, \dots, N$, leading to the univariate approximation

$$\hat{y}_1(\mathbf{X}) = \sum_{i=1}^N \sum_{j=1}^n \phi_j(X_i) y(c_1, \dots, c_{i-1}, x_i^{(j)}, c_{i+1}, \dots, c_N) - (N - 1)y(\mathbf{c}), \tag{11}$$

and to the bivariate approximation

$$\hat{y}_2(\mathbf{X}) \equiv \sum_{\substack{i_1, i_2=1 \\ i_1 < i_2}}^N \sum_{j_2=1}^n \sum_{j_1=1}^n \phi_{j_1}(X_{i_1}) \phi_{j_2}(X_{i_2}) y(c_1, \dots, c_{i_1-1}, x_{i_1}^{(j_1)}, c_{i_1+1}, \dots, c_{i_2-1}, x_{i_2}^{(j_2)}, c_{i_2+1}, \dots, c_N) - (N-2) \sum_{i=1}^N \sum_{j=1}^n \phi_j(X_i) y(c_1, \dots, c_{i-1}, x_i^{(j)}, c_{i+1}, \dots, c_N) + \frac{(N-1)(N-2)}{2} y(\mathbf{c}). \tag{12}$$

Following a similar consideration, the generalized S -variate approximation can be derived as

$$\hat{y}_S(\mathbf{X}) = \sum_{i=0}^S (-1)^i \binom{N-S+i-1}{i} \sum_{\substack{k_1, \dots, k_{S-i}=1 \\ k_1 < \dots < k_{S-i}}}^N \sum_{j_{S-i}=1}^n \dots \sum_{j_1=1}^n \phi_{j_1}(X_{k_1}) \dots \phi_{j_{S-i}}(X_{k_{S-i}}) \times y(c_1, \dots, c_{k_1-1}, x_{k_1}^{(j_1)}, c_{k_1+1}, \dots, c_{k_{S-i}-1}, x_{k_{S-i}}^{(j_{S-i})}, c_{k_{S-i}+1}, \dots, c_N), \tag{13}$$

which can be utilized to generate higher-variate approximations if desired. But, due to their higher cost, only univariate and bivariate approximations are considered in this paper. Nevertheless, Eq. (13) provides a convergent sequence of lower-variate approximations of $y(\mathbf{X})$.

4.3. Monte Carlo simulation

Once the Lagrange shape functions $\phi_j(x_i)$ and deterministic coefficients $y(\mathbf{c}), y(c_1, \dots, c_{i-1}, x_i^{(j)}, c_{i+1}, \dots, c_N), y(c_1, \dots, c_{i_1-1}, x_{i_1}^{(j_1)}, c_{i_1+1}, \dots, c_{i_2-1}, x_{i_2}^{(j_2)}, c_{i_2+1}, \dots, c_N)$, and $y(c_1, \dots, c_{k_1-1}, x_{k_1}^{(j_1)}, c_{k_1+1}, \dots, c_{k_{S-i}-1}, x_{k_{S-i}}^{(j_{S-i})}, c_{k_{S-i}+1}, \dots, c_N)$ are generated, Eqs. (11)–(13) provide explicit approximations of a crack-driving force in terms of random input \mathbf{X} . Therefore, any probabilistic characteristics of the crack-driving force, including its statistical moments and probability density function, can be easily evaluated by performing Monte Carlo simulation on Eqs. (11)–(13). Since Eqs. (11)–(13) do not require solving additional FEA, the embedded Monte Carlo simulation can be efficiently conducted for any sample size.

For fracture reliability analysis if $y(\mathbf{x})$ represents a performance function (see Section 2), the Monte Carlo estimate $P_{F,S}$ of the failure probability employing an S -variate approximation is

$$P_{F,S} = \frac{1}{N_S} \sum_{i=1}^{N_S} \mathbb{I}[\hat{y}_S(\mathbf{x}^{(i)}) < 0] \tag{14}$$

where $\mathbf{x}^{(i)}$ is the i th realization of \mathbf{X} , N_S is the sample size, and $\mathbb{I}[\cdot]$ is an indicator function such that $\mathbb{I} = 1$ if $\mathbf{x}^{(i)}$ is in the failure set (i.e., when $\hat{y}_S(\mathbf{x}^{(i)}) < 0$) and zero otherwise. By setting $S = 1$ or 2 , univariate or bivariate approximations can be invoked.

The proposed methods involving univariate (Eq. (11)) or bivariate (Eq. (12)) approximations, n -point Lagrange interpolation (Eq. (8) or (10)), and associated Monte Carlo simulation are defined as the *univariate* or *bivariate decomposition methods* in this paper. The methods developed do not require calculation of any partial derivatives of the crack-driving force as compared with the commonly-employed FORM/SORM in fracture reliability analysis [8–10].

4.4. Computational effort

The univariate and bivariate approximations require numerical function evaluations of $y(\mathbf{x})$ (e.g., linear or nonlinear FEA) to determine $y(\mathbf{c}), y(c_1, \dots, c_{i-1}, x_i^{(j)}, c_{i+1}, \dots, c_N)$, and $y(c_1, \dots, c_{i_1-1}, x_{i_1}^{(j_1)}, c_{i_1+1}, \dots, c_{i_2-1}, x_{i_2}^{(j_2)}, c_{i_2+1}, \dots, c_N)$ for $i, i_1, i_2 = 1, \dots, N$ and $j, j_1, j_2 = 1, \dots, n$. Hence, the computational effort required by the proposed method can be viewed as numerically solving a fracture-mechanics problem at several deterministic input defined by user-selected sample points. There are n and n^2 numerical evaluations of $y(\mathbf{x})$ involved in Eqs. (8) and (10), respectively. Therefore, the total cost for the univariate decomposition method entails a *maximum* of $nN + 1$ function evaluations, and for the bivariate approximation, $N(N-1)n^2/2 + nN + 1$ *maximum* function evaluations are required. If the selected sample points include a common

sample point in each coordinate x_i (see the following section), the numbers of functions evaluations reduce to $(n-1)N+1$ and $N(N-1)(n-1)^2/2 + (n-1)N+1$ for univariate and bivariate methods, respectively.

5. Numerical examples

Three numerical examples involving linear-elastic and nonlinear fracture mechanics of two- and three-dimensional cracked structures are presented to illustrate the dimensional decomposition method. Whenever possible, comparisons have been made with the commonly-used FORM and the direct Monte Carlo simulation to evaluate the accuracy and efficiency of the proposed method.

In all three examples, the function decomposition was formulated in the Gaussian image (\mathbf{u} space) of the original space (\mathbf{x} space) of random input. The reference point \mathbf{c} associated with the decomposition method was fixed at the mean input in the \mathbf{u} space. A 5-point (i.e., $n=5$) Lagrange interpolation was selected. In the \mathbf{u} space, sample points $(c_1, \dots, c_{i-1}, u_i^{(j)}, c_{i+1}, \dots, c_N)$ and $(c_1, \dots, c_{i-1}, u_{i_1}^{(j_1)}, c_{i_1+1}, \dots, c_{i_2-1}, u_{i_2}^{(j_2)}, c_{i_2+1}, \dots, c_N)$ were chosen with $c_i=0$. In Example 1, fifth-order Gauss–Hermite integration points were employed for defining $u_i^{(j)}$ or $u_{i_1}^{(j_1)}$ or $u_{i_2}^{(j_2)}$. In Examples 2 and 3, uniformly distributed points $u_i^{(j)}$ or $u_{i_1}^{(j_1)}$ or $u_{i_2}^{(j_2)} = -2, -1, 0, 1, 2$ were deployed. Regardless of the distribution of sample points chosen, $(n-1)N+1$ and $(n-1)^2N(N-1)/2 + (n-1)N+1$ function evaluations are involved in univariate and bivariate methods, respectively, in all three examples.

5.1. Example 1: A linear-elastic and isotropic functionally graded plate

The first example involves a two-dimensional, edge-cracked plate made of a linear-elastic and isotropic functionally graded material (FGM), presented to illustrate a mixed-mode probabilistic fracture-mechanics analysis using the proposed decomposition method. As shown in Fig. 1(a), an FGM plate of length $L=16$ in was fixed at the bottom and subjected to a stochastic far-field normal stress σ^∞ and a shear stress τ^∞ applied at the top. The elastic modulus was assumed to vary smoothly according to

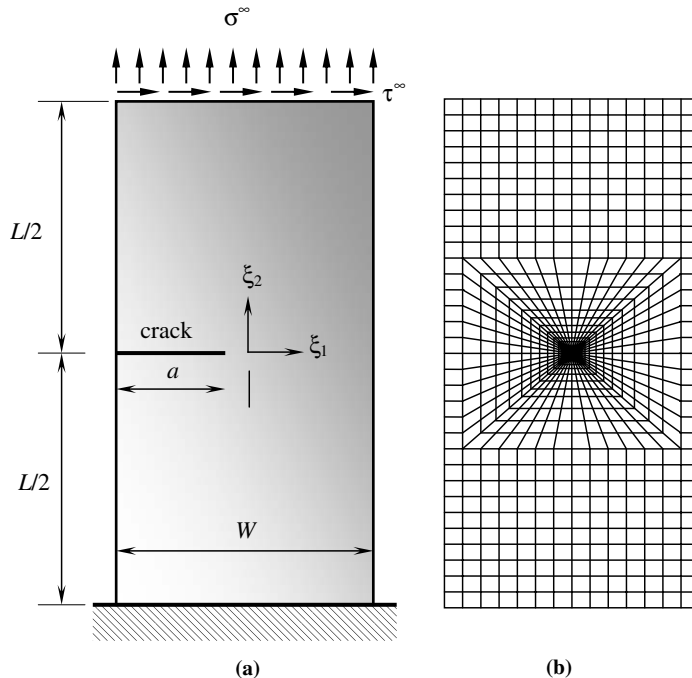


Fig. 1. An FGM edge-cracked plate: (a) geometry and loads and (b) finite-element discretization at mean crack size.

Table 1
Statistical properties of random input for the FGM plate

Random variable	Mean	Standard deviation	Probability distribution
Crack length (a), in	3.5	0.404	Uniform ^a
Plate width (W), in	7.5	0.289	Uniform ^b
Far-field tensile stress (σ^∞), ksi	1	0.1	Gaussian
Far-field shear stress (τ^∞), ksi	1	0.1	Gaussian
Modulus angle parameter (θ), rad	0	0.1	Gaussian
Modulus parameter (E_1), ksi	1	0.1	Lognormal
Modulus parameter (E_2), ksi	3	0.3	Lognormal
Modulus gradation parameter (β), in ⁻¹	μ_β^c	0.1 μ_β^c	Lognormal

^a Uniformly distributed over (2.8 in, 4.2 in).

^b Uniformly distributed over (7 in, 8 in).

^c μ_β varies as 0, 1, and 5 in⁻¹.

$$E(\xi_1, \xi_2) = \frac{E_1 + E_2}{2} + \frac{E_1 - E_2}{2} \tanh[\beta(\xi_1 \cos \theta + \xi_2 \sin \theta)], \tag{15}$$

where (ξ_1, ξ_2) are spatial coordinates with the center of the plate as the origin, E_1, E_2, β , and θ are modulus parameters. A plane strain condition was assumed. The Poisson’s ratio $\nu = 0$. The following eight independent random variables are defined: (1) crack length a ; (2) plate width W ; (3) far-field normal stress σ^∞ ; (4) far-field shear stress τ^∞ ; (5) modulus angle parameter $-\pi/2 \leq \theta \leq \pi/2$; (6) modulus parameter $E_1 = E(\infty, \xi_2)$; (7) modulus parameter $E_2 = E(-\infty, \xi_2)$; and (8) modulus gradation parameter β . The statistical property of the random input $\mathbf{X} = \{a, W, \sigma^\infty, \tau^\infty, \theta, E_1, E_2, \beta\}^T \in \mathbb{R}^8$ is defined in Table 1. The gradation parameter β has mean values $\mu_\beta = 0, 1$, and 5 in^{-1} with a standard deviation $\sigma_\beta = 0.1\mu_\beta$.

Due to the far-field normal stress σ^∞ and shear stress τ^∞ , the plate is subjected to mixed-mode deformation involving fracture modes I and II. The mixed-mode stress-intensity factors $K_I(\mathbf{X})$ and $K_{II}(\mathbf{X})$ were calculated using an interaction integral method [15]. The plate was analyzed using the finite element method involving a total of 832 8-noded, regular, quadrilateral elements and 48 6-noded, quarter-point (singular), triangular elements at the crack-tip, as shown in Fig. 1(b).

Fig. 2 displays the variation of the elastic modulus in Eq. (15) with respect to ξ_1 when $E_1 = 1 \text{ ksi}$, $E_2 = 3 \text{ ksi}$, $W = 7.5 \text{ in}$, $\beta = 0, 0.3, 1$, and 5 in^{-1} , and the material gradation follows horizontally (i.e., $\theta = 0$). The gradation parameter $\beta > 0$, which represents a truly FGM plate, controls the smoothness of transition between the elastic moduli at two ends of the plate. When β increases, the smoothness decreases, as depicted in Fig. 2.

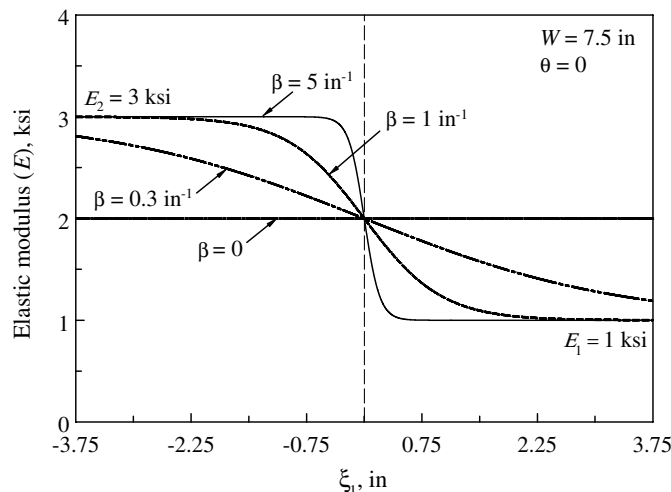


Fig. 2. Variation of elastic modulus for several gradation parameters.

When $\beta \rightarrow \infty$, the plate is no longer FGM and the transition occurs as a step function at $\xi_1 = 0$. When $\beta = 0$, the plate is homogeneous with the elastic modulus taking on a constant average value of $(E_1 + E_2)/2 = 2$ ksi. Hence, several scenarios of the elastic modulus gradation can be created by appropriately varying β .

For the FGM plate, the failure criterion is based on a mixed-mode fracture initiation using the maximum tangential stress theory [16], which leads to the performance function

$$y(\mathbf{X}) = K_{Ic} - K_{eff}(\mathbf{X}) = K_{Ic} - \left[K_I(\mathbf{X}) \cos^2 \frac{\Theta(\mathbf{X})}{2} - \frac{3}{2} K_{II}(\mathbf{X}) \sin \Theta(\mathbf{X}) \right] \cos \frac{\Theta(\mathbf{X})}{2}, \tag{16}$$

where K_{Ic} is a deterministic mode-I fracture toughness, typically measured from small-scale fracture experiments under a plane strain condition, and

$$\Theta_c(\mathbf{X}) = \begin{cases} 2 \tan^{-1} \left(\frac{1 - \sqrt{1 + 8[K_{II}(\mathbf{X})/K_I(\mathbf{X})]^2}}{4K_{II}(\mathbf{X})/K_I(\mathbf{X})} \right), & \text{if } K_{II}(\mathbf{X}) > 0 \\ 2 \tan^{-1} \left(\frac{1 + \sqrt{1 + 8[K_{II}(\mathbf{X})/K_I(\mathbf{X})]^2}}{4K_{II}(\mathbf{X})/K_I(\mathbf{X})} \right), & \text{if } K_{II}(\mathbf{X}) < 0 \end{cases} \tag{17}$$

is the direction of crack propagation. For $\mu_\beta = 5 \text{ in}^{-1}$ and $\sigma_\beta = 0.1 \mu_\beta = 0.5 \text{ in}^{-1}$, the probability of fracture initiation $P_F = P[y(\mathbf{X}) < 0]$, predicted using the proposed univariate and bivariate decomposition methods, FORM, and the direct Monte Carlo simulation, is plotted in Fig. 3 as a function of fracture toughness K_{Ic} . All methods predict lower failure probability for higher toughness, as expected. Using $n = 5$ and $N = 8$, the univariate and bivariate methods require only 33 and 481 functions evaluations (FEA), respectively, whereas 10^5 FEA were performed by the direct Monte Carlo simulation. The reliability analysis by FORM requires 50–100 FEA depending on the value of fracture toughness considered in this example. The results clearly show that both the univariate and bivariate methods developed in this work can calculate the probability of fracture initiation accurately and efficiently. Due to the high nonlinearity of the performance function associated with FGM, FORM, which is commonly used in reliability analysis, may overestimate probability of fracture initiation significantly.

Fig. 4 presents the failure probability vs. fracture toughness plots obtained by the bivariate decomposition method for several values of mean gradation parameter: $\mu_\beta = 0, 1, \text{ and } 5 \text{ in}^{-1}$ ($\sigma_\beta = 0.1 \mu_\beta$ in all three cases). For FGM ($\mu_\beta > 0$), the failure probability decreases when μ_β decreases, indicating that a smoother transition of material property lowers failure probability; the reduction of the failure probability is significant at higher thresholds of fracture toughness. When $\mu_\beta = 0$, the plate is homogeneous (i.e., a degenerate case) with a constant and average elastic modulus with no gradation and the failure probability trend reaches the lowest possible value.

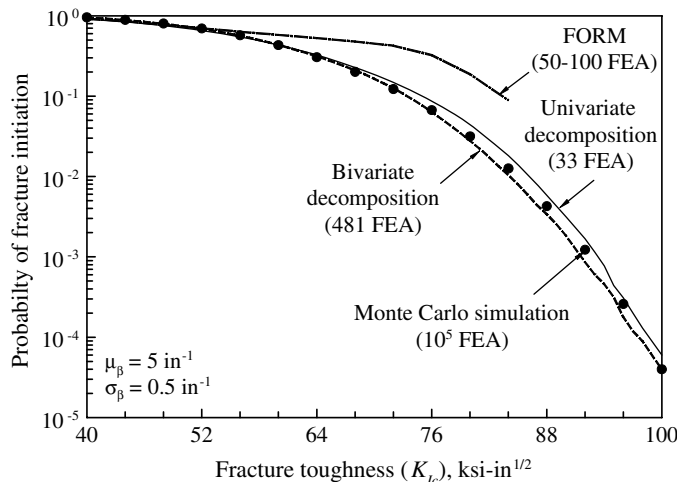


Fig. 3. Probability of fracture initiation for the FGM plate.

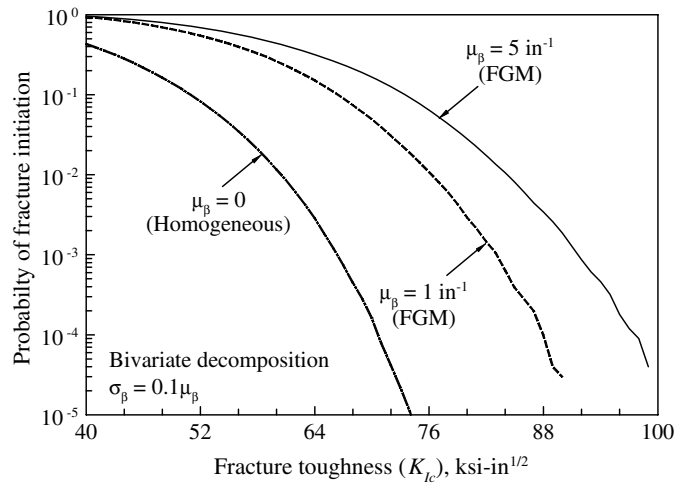


Fig. 4. Effect of gradation parameter on the probability of fracture initiation.

5.2. Example 2: A nonlinear double-edged-notched tension specimen

Consider a two-dimensional, homogeneous, double-edged-notched tension [DE(T)] specimen with width $2W = 40$ in, length $2L = 200$ in, and random crack length a , subject to a random far-field tensile stress σ^∞ , as shown in Fig. 5(a). The nonlinear-elastic constitutive equation under small-displacement condition is based on the well-known Ramberg–Osgood relation [16]

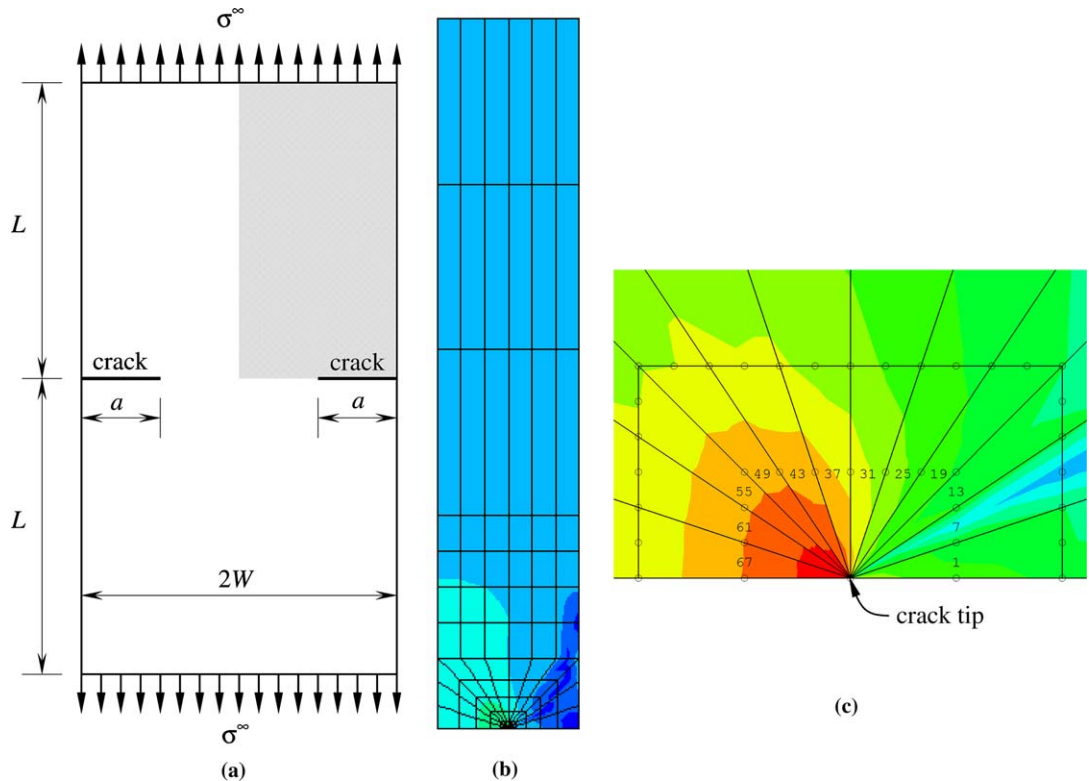


Fig. 5. A DE(T) specimen: (a) geometry and loads, (b) finite-element discretization at mean crack size, and (c) singular elements at the crack tip.

Table 2
Statistical properties of random input for the DE(T) specimen

Random variable	Mean	Coefficient of variation	Probability distribution
Crack length (a), in	10	0.1	Lognormal
Elastic modulus (E), psi	30×10^6	0.05	Gaussian
Ramberg–Osgood coefficient (α)	10	0.1	Lognormal
Ramberg–Osgood exponent (m)	5	0.1	Lognormal
Far-field tensile stress (σ^∞), psi	$\mathbb{E}[\sigma^\infty]^a$	0.05	Gaussian

^a $\mathbb{E}[\sigma^\infty]$ represents mean of σ^∞ and varies as 10,000 psi (Case 1) and 18,000 psi (Case 2).

$$\varepsilon_{ij} = \frac{1 + \nu}{E} s_{ij} + \frac{1 - 2\nu}{3E} \sigma_{kk} \delta_{ij} + \frac{3}{2E} \alpha \left(\frac{\sigma_e}{\sigma_0} \right)^{m-1} s_{ij}, \quad (18)$$

where σ_{ij} and ε_{ij} are stress and strain components, respectively, E is the Young's modulus, ν is the Poisson's ratio, σ_0 is a reference stress, α is a dimensionless material coefficient, m is the strain hardening exponent, δ_{ij} is the Kronecker delta, $s_{ij} = \sigma_{ij} - 1/3 \sigma_{kk} \delta_{ij}$ is the deviatoric stress, and $\sigma_e = \sqrt{3/2} s_{ij} s_{ij}$ is the von Mises equivalent stress. For nonlinear-elastic cracked structures, the J -integral uniquely defines the asymptotic crack-tip stress and strain fields, known as the Hutchinson–Rice–Rosengren singularity field [16]. The far-field stress σ^∞ , crack length a , and material constants E , α , and m were treated as statistically independent random variables. Table 2 presents the mean, coefficient of variation, and probability distribution for each of these random parameters. The Poisson's ratio of $\nu = 0.3$ was assumed to be deterministic. Two load cases involving a low mean value of the applied stress $\mathbb{E}[\sigma^\infty] = 10,000$ psi (Case 1) and a high mean value of the applied stress $\mathbb{E}[\sigma^\infty] = 18,000$ psi (Case 2) were studied.

Due to the double-symmetry of this DE(T) problem, Fig. 5(b) shows a finite element mesh (at mean crack length) of the 1/4-model. A total of 114 elements and 393 nodes were used in the mesh. Both plane stress and plane strain conditions were studied. Second-order elements from the ABAQUS (Version 6.5) [17] element library were employed. For plane stress, the element type was CPS8R – the reduced integration, eight-noded quadrilateral element. The element type CPE8R was used for plane strain. Focused singular elements were deployed in the vicinity of the crack tip (Fig. 5(c)). A 2×2 Gaussian integration rule was employed in FEA.

Fig. 6 shows the deterministic, nonlinear FEA results of the J -integral obtained as a function of the far-field stress σ^∞ for both plane stress and plane strain conditions. The mean values of crack length and material

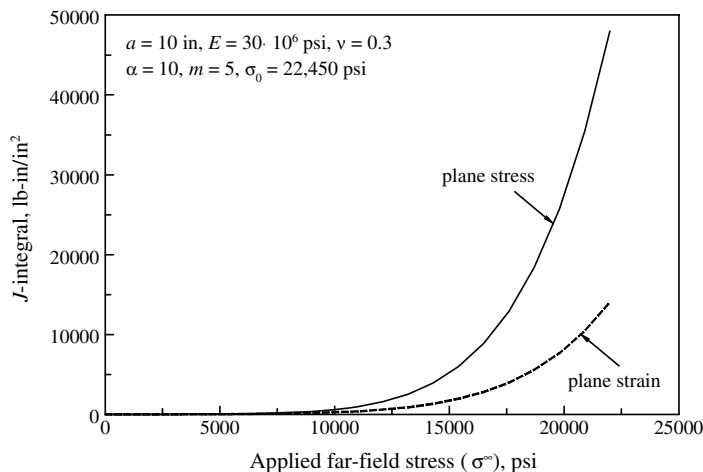


Fig. 6. J -integral for various far-field applied stress.

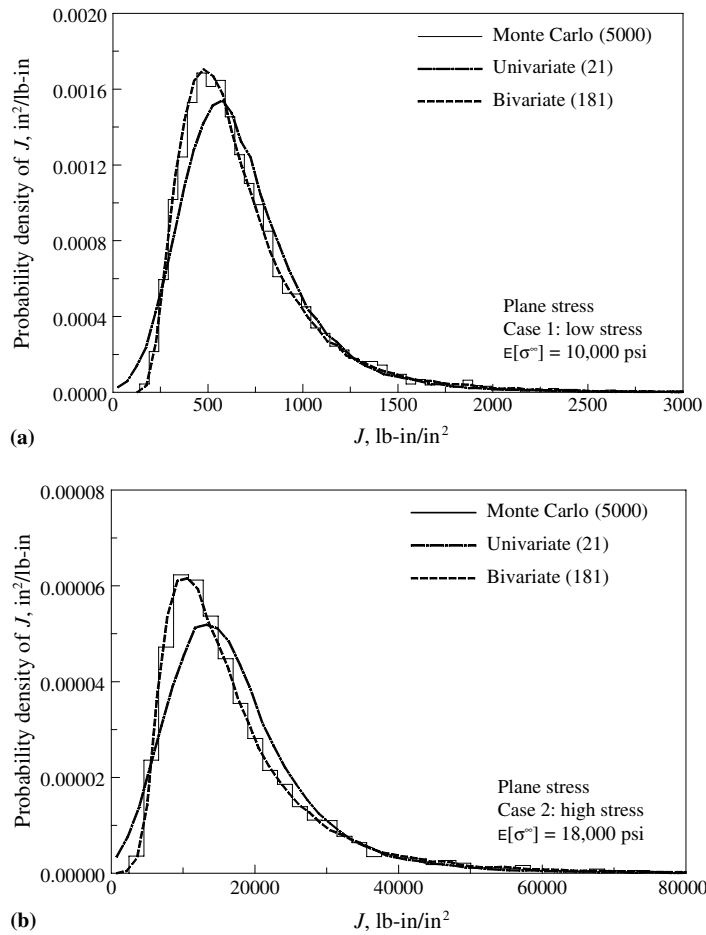


Fig. 7. Probability density of J for DE(T) specimen in plane stress: (a) Case 1 and (b) Case 2.

properties defined in Table 2 were employed to generate the plots in Fig. 6. The crack-driving force (J -integral) for a given applied stress is higher for plane stress than that for plane strain.

Fig. 7(a) and (b) shows comparisons of predicted probability densities and/or histograms of the J -integral under plane stress condition by the univariate and bivariate decomposition methods and the direct Monte Carlo simulation. Due to expensive FEA (ABAQUS analysis), only 5000 samples of J were generated in the direct Monte Carlo simulation. Results of two load cases involving $E[\sigma^\infty] = 10,000$ psi (Case 1) and $E[\sigma^\infty] = 18,000$ psi (Case 2) are shown in Fig. 7(a) and (b), respectively. In each case, the decomposition method, which entails Monte Carlo analysis employing the univariate or bivariate approximations in Eq. (11) or (12), permits inexpensive calculation of the J -integral by sidestepping additional nonlinear FEA solutions. Hence, an arbitrarily large sample size of the embedded Monte Carlo analysis, such as 100,000 in this particular example, was selected to generate the probability densities of J by the decomposition method. Compared with the direct Monte Carlo simulation, the univariate method retaining only individual effects of random variables yields encouraging results. The bivariate method, which includes both individual and cooperative effects of random variables, provides excellent estimates of the probability densities of the J -integral. Similar analyses under a plane strain condition, which were conducted for the above-mentioned two load cases and leading to the results of Fig. 8(a) and (b), reveal the same qualitative trend, except the J -integral values for plane strain are much lower than that in plane stress, as deterministically observed in Fig. 6. Using $n = 5$ and $N = 5$, the univariate and bivariate decomposition methods involve only 21 and 181 functions evaluations (FEA), respectively, whereas 5000 FEA were performed by the direct Monte Carlo simulation. Therefore, the method developed is not only accurate, but also computationally efficient.

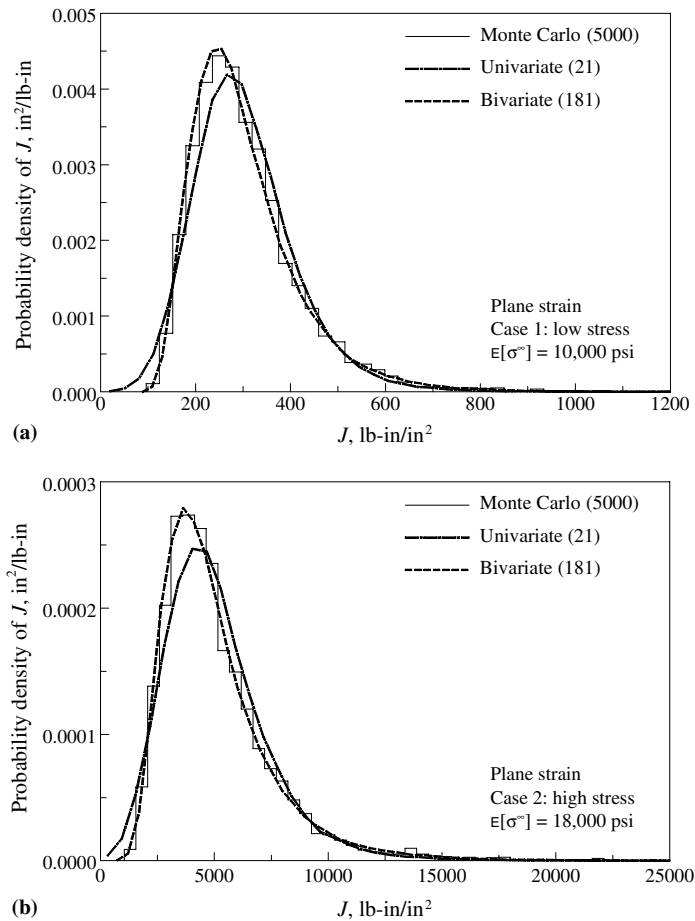


Fig. 8. Probability density of J for DE(T) specimen in plane strain: (a) Case 1 and (b) Case 2.

5.3. Example 3: A nonlinear through-walled-cracked cylinder

The final example of the paper involves nonlinear fracture-mechanics analysis of a three-dimensional, circumferential, through-wall-cracked (TWC) cylinder subjected to four-point bending, as shown in Fig. 9(a). The cylinder has a mid-thickness radius $R = 50.8$ mm, a wall thickness $t = 5.08$ mm, and a symmetrically centered through-wall crack with the normalized crack angle $\theta/\pi = 0.125$. The outer span $L = 1.5$ m and the inner span $S = 0.6$ m. The cylinder is composed of ASTM Type 304 stainless steel with an operating temperature of 288 C. The cross-sectional geometry at the cracked section is shown in Fig. 9(b). TWC cylinders like the one in Example 3 are frequently analyzed for fracture evaluation of pressure boundary integrity in the nuclear industry.

Table 3 lists the means, coefficients of variation, and probability distributions of tensile parameters (E, α, m), four-point bending load (P), and fracture toughness (J_{Ic}). The statistics of the material properties were obtained from actual Type 304 stainless steel data at 288 C [18]. However, the probabilistic characteristics of P were chosen arbitrarily. The load has a mean value μ_P that varies from 23.2 – 64 kN, but with a standard deviation $\sigma_P = 0.1 \mu_P$ in each load case. All random variables are statistically independent. Also, $\sigma_0 = 154.78$ MPa and $\nu = 0.3$.

A finite element mesh of the quarter model of the TWC cylinder is shown in Fig. 9(c). Twenty-noded isoparametric solid elements (C3D20R) from the ABAQUS library were used, with focused singular elements at the crack tip. A total of 236 elements and 1805 nodes were created. The stress–strain curve was modeled using the nonlinear Ramberg–Osgood equation (Eq. (18)) in this example as well.

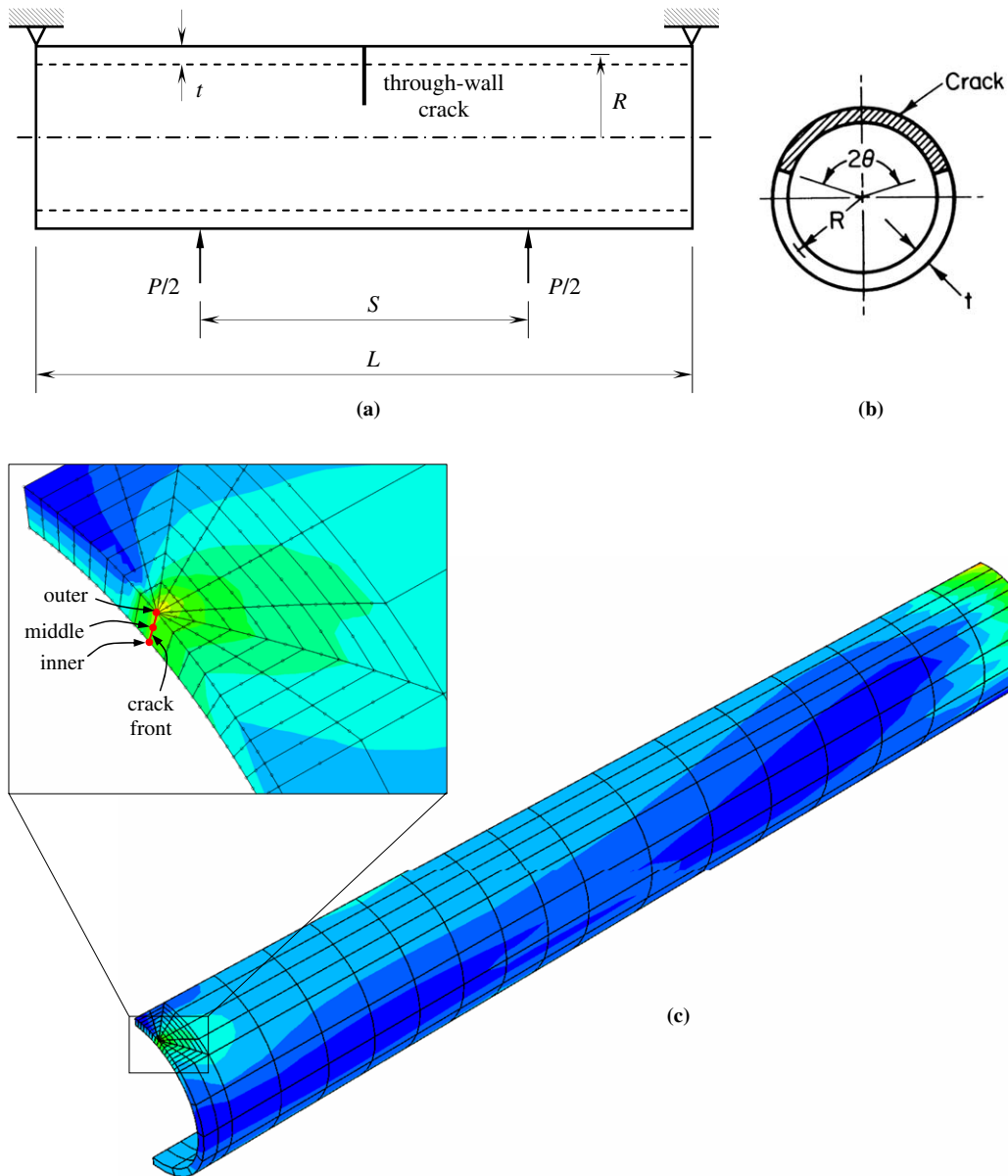


Fig. 9. ATWC cylinder under four-point bending: (a) geometry and loads, (b) cracked cross-section, and (c) finite-element discretization.

Table 3
Statistical properties of random input for the TWC cylinder

Random variable	Mean	Coefficient of variation	Probability distribution
Elastic modulus (E), GPa	182.7	0.1	Gaussian
Ramberg–Osgood coefficient (α)	8.073	0.439	Lognormal
Ramberg–Osgood exponent (m)	3.8	0.146	Lognormal
Four-point bending load (P), kN	μ_P^a	0.1	Gaussian
Initiation toughness (J_{Ic}), kJ/m ²	1242.6	0.47	Lognormal

^a μ_P varies as 23.2, 25.6, 28, 30.4, 33.6, 36, 38.4, 41.6, 45.6, 56, and 64 kN.

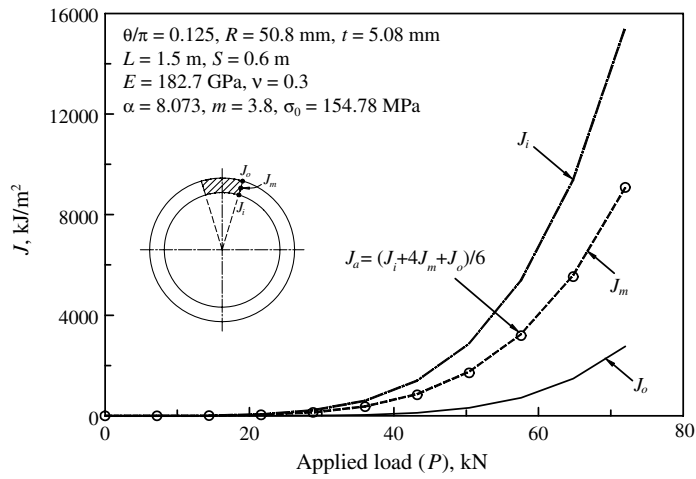


Fig. 10. J -integrals for the TWC cylinder under pure bending at various crack tips.

Fig. 10 displays the J -integral vs. load P plots using the mean values of random material properties defined in Table 3. The variations of J -integrals at the outer crack tip (J_o), middle crack tip (J_m), and inner crack tip

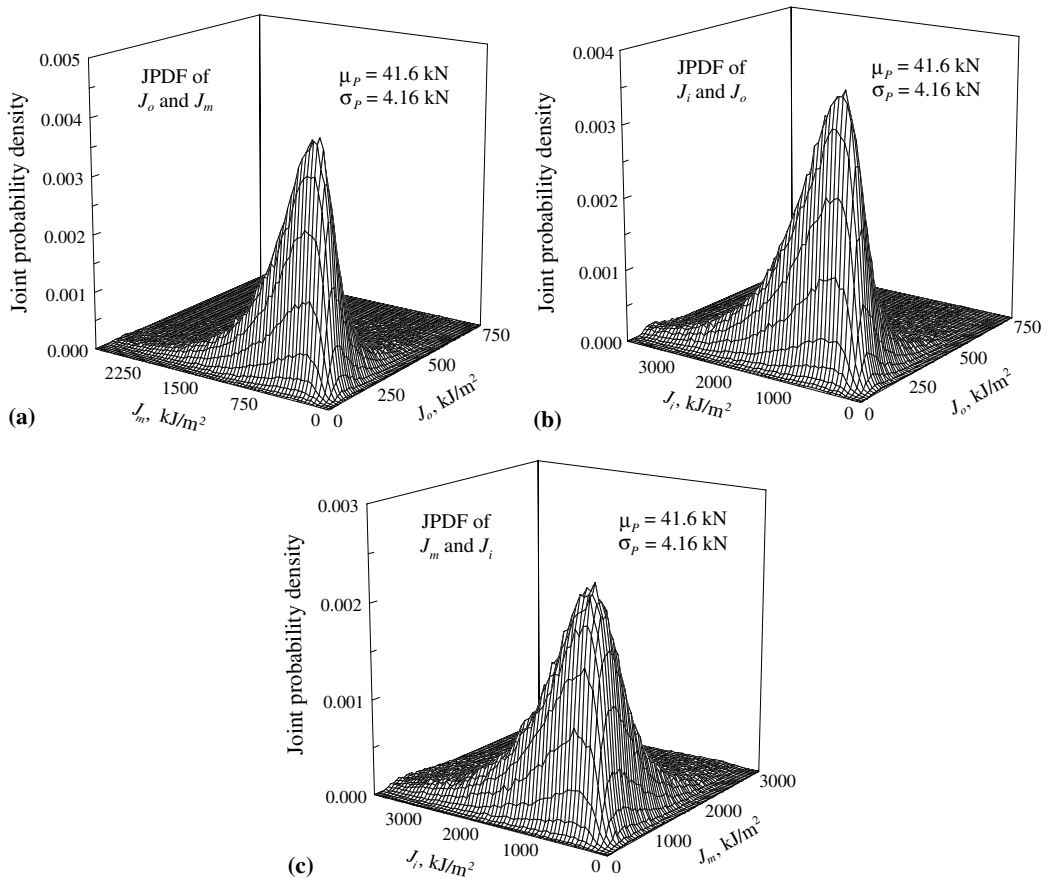


Fig. 11. Joint probability densities of J -integrals for $\mu_p = 41.6$ kN at various crack tips: (a) J_o and J_m , (b) J_o and J_i , and (c) J_i and J_m .

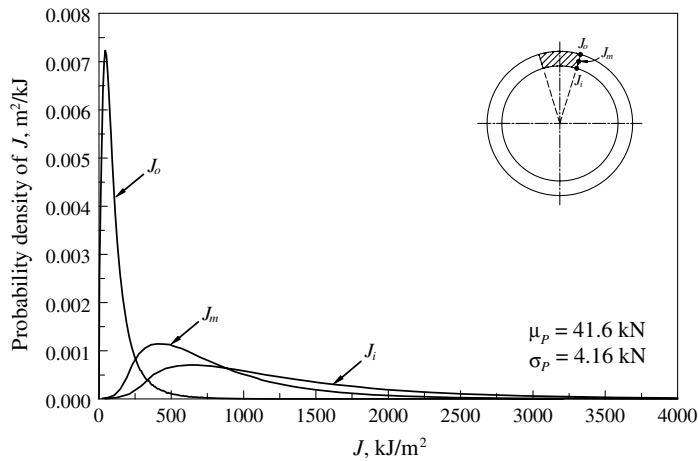


Fig. 12. Marginal probability densities of J -integrals for $\mu_p = 41.6$ kN.

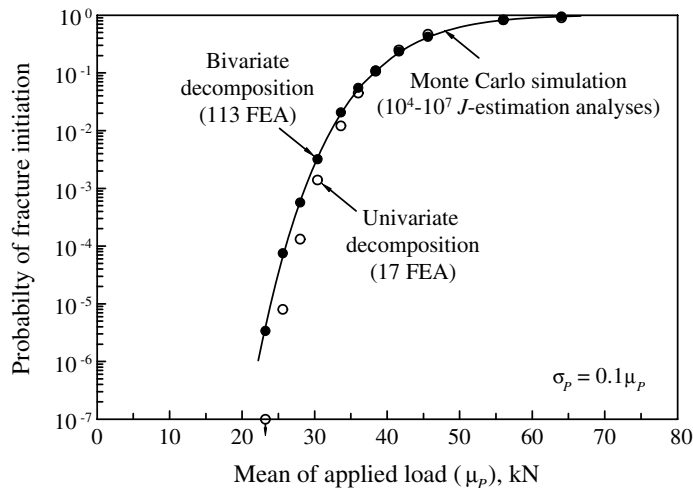


Fig. 13. Probability of fracture initiation of the TWC cylinder.

(J_i), plotted individually, show the through-the-thickness variation of J . The weighted-average $J_a \equiv (J_i + 4J_m + J_o)/6$ appears to be close to J_m .

Using Monte Carlo simulation (10^6 samples) on Eq. (12), Fig. 11(a)–(c) present joint probability densities of three J -integral pairs $\{J_o, J_m\}$, $\{J_o, J_i\}$, and $\{J_i, J_m\}$ by the bivariate decomposition method when $\mu_p = 41.6$ kN and $\sigma_p = 0.1 \mu_p = 4.16$ kN. Using $n = 5$ and $N = 4^1$, only 113 nonlinear FEA were required by the bivariate method. The marginal probability densities of J_o , J_m , and J_i were also calculated and are exhibited in Fig. 12.

Finally, the probability of fracture initiation in the TWC cylinder, defined as $P_F = P[J_{Ic}(\mathbf{X}) - J_a(\mathbf{X}) < 0]$, was calculated for mean applied load μ_p varying between 23.2 and 64 kN ($\sigma_p = 0.1 \mu_p$ in all load cases) and is presented in Fig. 13. Both univariate (open circle) and bivariate (closed circle) decomposition methods involving 10^4 – 10^7 samples in the embedded Monte Carlo analysis (depending on P_F) were employed to generate the failure probability plots. Due to expensive FEA, direct Monte Carlo simulation was not feasible for this example to verify low probabilities in Fig. 13. Instead, a J -estimation-based Monte Carlo simulation [19] (solid line) involving 10^4 – 10^7 samples (depending on P_F) was also performed, the results of which are

¹ The J -integral depends on four random variables E , α , m , and P and does not depend on material resistance J_{Ic} .

displayed in Fig. 13. Decomposition methods, in particular the bivariate version, provide excellent estimates of the probability of fracture initiation in cracked cylinders.

6. Conclusions

A dimensional decomposition method was developed for obtaining probabilistic characteristics of crack-driving forces and reliability analysis of general cracked structures subject to random loads, material properties, and crack geometry. The method is based on (1) a novel function decomposition allowing lower-variate approximations of a crack-driving force or a performance function; (2) Lagrange interpolations for representing lower-variate component functions, and (3) Monte Carlo simulation. The proposed decomposition results in a finite, hierarchical, and convergent series for a crack-driving force or a performance function of interest. The computational effort in finding the probabilistic characteristics of the crack-driving force or reliability analysis can be viewed as performing deterministic fracture analyses at selected input defined by sample points. Compared with commonly-used FORM/SORM, no derivatives of fracture response parameters are required by the new method developed. Hence, the method can be easily adapted for solving a general probabilistic fracture-mechanics problem involving third-party commercial finite-element codes. Results of three numerical examples involving two-dimensional linear-elastic fracture of a functionally-graded plate and non-linear fracture of two- and three-dimensional cracked structures indicate that the decomposition method provides excellent estimates of probability densities of the J -integral and probability of fracture initiation for various cases including material gradation characteristics and magnitudes of applied stresses and loads. The computational efforts required by the univariate and bivariate versions of the decomposition method are linear and quadratic with respect to the number of random variables involved. Therefore, the method developed is accurate and computationally efficient when compared with FORM and direct Monte Carlo simulation.

Acknowledgement

The author would like to acknowledge the financial support by the US National Science Foundation under Grant No. DMI-0355487.

References

- [1] Madsen HO, Krenk S, Lind NC. Methods of structural safety. Englewood Cliffs, NJ: Prentice-Hall, Inc.; 1986.
- [2] Rackwitz R. Reliability analysis – a review and some perspectives. Struct Safety 2001;23(4):365–95.
- [3] Ditlevsen O, Madsen HO. Structural reliability methods. Chichester: John Wiley & Sons Ltd.; 1996.
- [4] Rubinstein RY. Simulation and the Monte Carlo method. New York: John Wiley & Sons; 1981.
- [5] Niederreiter H, Spanier J. Monte Carlo and quasi-Monte Carlo methods. Berlin: Springer-Verlag; 2000.
- [6] Melchers RE. Importance sampling in structural systems. Struct Saf 1989;6:3–10.
- [7] Chen G, Rahman S, Park YH. Shape sensitivity analysis in mixed-mode fracture mechanics. Comput Mech 2001;27(4):282–91.
- [8] Chen G, Rahman S, Park YH. Shape sensitivity and reliability analyses of linear-elastic cracked structures. Int J Fract 2001;112(3):223–46.
- [9] Rahman S, Chen G. Continuum shape sensitivity and reliability analyses of nonlinear cracked structures. Int J Fract 2005;131(2):189–209.
- [10] Rahman S. A stochastic model for elastic-plastic fracture analysis of circumferential through-wall-cracked pipes subject to bending. Engng Fract Mech 1995;52(2):265–88.
- [11] Xu H, Rahman S. Decomposition methods for structural reliability analysis. Probabilis Engng Mech 2005;20:239–50.
- [12] Sobol IM. Theorems and examples on high dimensional model representations. Reliab Engng Syst Saf 2003;79:187–93.
- [13] Rabitz H, Alis OF, Shorter J, Shim K. Efficient input–output model representation. Comput Phys Commun 1999;117:11–20.
- [14] Xu H, Rahman S. A generalized dimension-reduction method for multi-dimensional integration in stochastic mechanics. Int J Numer Methods Engng 2004;61:1992–2019.
- [15] Rao BN, Rahman S. Meshfree analysis of cracks in isotropic functionally graded materials. Engng Fract Mech 2003;70(1):1–27.
- [16] Anderson TL. Fracture mechanics: fundamentals and applications. second ed. Boca Raton, Florida: CRC Press Inc.; 1995.
- [17] ABAQUS, User's guide and theoretical manual, version 6.5, Hibbit, Karlsson, and Sorenson, Inc., Pawtucket, RI, 2005.
- [18] Rahman S, Ghadiali N, Paul D, Wilkowski G. Probabilistic pipe fracture evaluations for leak-rate-detection applications. Topical report, NUREG/CR-6004, US Nuclear Regulatory Commission, Washington, DC, April 1995.
- [19] Rahman S. Probabilistic fracture mechanics: J -estimation and finite element methods. Engng Fract Mech 2000;68:107–25.